Electronic structure investigations of 4-aminophthal hydrazide by UV–visible, NMR spectral studies and HOMO–LUMO analysis by ab initio and DFT calculations

ARTICLE *in* SPECTROCHIMICA ACTA PART A MOLECULAR AND BIOMOLECULAR SPECTROSCOPY · MARCH 2015

Impact Factor: 2.35 · DOI: 10.1016/j.saa.2015.03.012 · Source: PubMed

3 AUTHORS, INCLUDING:

Kuppusamy Sambathkumar

A.A.Govt College-villupuram

7 PUBLICATIONS **15** CITATIONS

SEE PROFILE

Manivannan Arivazhagan

Government Arts College ,Thiruverumbur, …

60 PUBLICATIONS **335** CITATIONS

SEE PROFILE

Spectrochimica Acta Part A: Molecular and Biomolecular Spectroscopy 147 (2015) 124–138

Contents lists available at ScienceDirect

Spectrochimica Acta Part A: Molecular and Biomolecular Spectroscopy

journal homepage: www.elsevier.com/locate/saa

Electronic structure investigations of 4-aminophthal hydrazide by UV–visible, NMR spectral studies and HOMO–LUMO analysis by *ab initio* and DFT calculations

K. Sambathkumar [a,*], S. Jeyavijayan [b], M. Arivazhagan [c]

[a] P.G.&Research Department of Physics, A.A. Govt. Arts College, Villupuram 605602, India
[b] Department of Physics, J.J. College of Engineering and Technology,Tiruchirappalli 620 009, India
[c] Department of Physics, Government Arts College, Tiruchirappalli 620 022, India

HIGHLIGHTS

- The APH was characterized by FT-IR, FT-Raman, NMR and UV spectroscopy.
- Quantum chemical calculations were done by DFT method.
- The global minimum energy between the two methods shows the difference in optimizations.
- The TED calculation provides a strong support for the frequency assignment.
- HOMO, LUMO energies and MEP distribution of APH were performed.

GRAPHICAL ABSTRACT

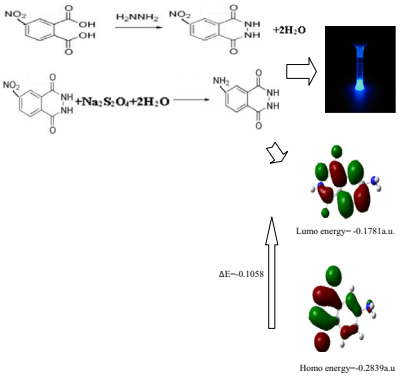

ARTICLE INFO

Article history:
Received 14 October 2014
Received in revised form 9 February 2015
Accepted 1 March 2015
Available online 24 March 2015

Keywords:
FTIR
FT-Raman
HOMO-LUMO
NMR
UV
MEP

ABSTRACT

Combined experimental and theoretical studies were conducted on the molecular structure and vibrational spectra of 4-AminoPhthalhydrazide (APH). The FT-IR and FT-Raman spectra of APH were recorded in the solid phase. The molecular geometry and vibrational frequencies of APH in the ground state have been calculated by using the *ab initio* HF (Hartree–Fock) and density functional methods (B3LYP) invoking 6-311+G(d,p) basis set. The optimized geometric bond lengths and bond angles obtained by HF and B3LYP method show best agreement with the experimental values. Comparison of the observed fundamental vibrational frequencies of APH with calculated results by HF and density functional methods indicates that B3LYP is superior to the scaled Hartree–Fock approach for molecular vibrational problems. The difference between the observed and scaled wave number values of most of the fundamentals is very small. A detailed interpretation of the NMR spectra of APH was also reported. The theoretical spectrograms for infrared and Raman spectra of the title molecule have been constructed. UV–vis spectrum of the compound was recorded and the electronic properties, such as HOMO and LUMO energies, were performed by time dependent density functional theory (TD-DFT) approach. Finally the calculations results were applied to simulated infrared and Raman spectra of the title compound which show good agreement with observed spectra. And the temperature dependence of the thermodynamic properties of constant pressure (C_p), entropy (S) and enthalpy change ($\Delta H0 \rightarrow T$) for APH were also determined.

* Corresponding author. Tel.: +91 9994188861.
E-mail address: sa75kumar@yahoo.co.in (K. Sambathkumar).

http://dx.doi.org/10.1016/j.saa.2015.03.012
1386-1425/

Introduction

Hydrazides and hydrazones, the acylated derivatives [1] of hydrazine besides being useful for a number of biological properties, hydrazides are important starting material for a wide range of derivatives utilizable in pharmaceutical products and as surfactants. The hydrazones derivatives are used for fungicides, and in the treatment such as tuberculosis, leprosy and mental disorders. Biological assessment of fatty hydrazide and the derivatives have been the focus of earlier investigative studies [2,3]. The fatty hrdrazides are further derivatives to obtain new anti bacterial and anti fungal agents. Acylhydrazones, as an example of Schiff bases, and their metal complexes have widely studied due to their versatile applications in the fields of analytical and medicinal chemistry and biotechnology [4–6]. *p*-Hydroxy benzohydrazide moiety and its analogs seemed to be suitable parent compounds upon which variety of biological activities are reported such as antitumor [7,8], antianginal [9], antitubercular [10], antihypertensive [11] and antibacterial [12]. Hydrazides have recently become attractive to theoreticians as well as experimentalists due to the biological significance particularly in medicinal and enzyme chemistry. Harmonic force fields of polyatomic molecule play a vital role in the interpretation of vibrational spectra and in the prediction of other vibrational properties. Many substituted hydrazides are employed in the treatment of psychotic and psychoneurotic conditions. Carboxylic acid hydrazides are known to exhibit strong antibacterial activities which are enhanced by complexation with metal ions. The vibrational spectral studies of hydrazone is analyzed by Durig et al. [13]. The FTIR and FT-Raman spectra of 4-AminoPhthalohydrazide, and carried out normal coordinate calculations using classical method developed by Wilson to support the vibrational analysis [14]. To our knowledge, literature survey also reveals that to the best of our knowledge no theoretical calculations or detailed vibrational infrared and Raman analysis have been performed on APH molecule so far. A systematic study on the vibrational spectra and structure will aid in understanding the vibrational modes of this title molecule. So, in this work, the vibrational wave numbers, geometrical parameters, modes of vibrations, minimum energy, ^{1}H and ^{13}C NMR chemical shifts are calculated with GIAO approach by applying B3LYP method and electrostatic potential also provide information about electronic effects of APH molecule were investigated by using *ab initio* HF and B3LYP calculations with 6-311+G(d,p) basis set. And the electronic dipole moment (μ) and the first hyperpolarizability (β) value of the investigate molecule computed show that the APH molecule might have microscopic nonlinear optical (NLO) behavior with non-zero values. The UV spectroscopic studies along with HOMO, LUMO analysis have been used to elucidate information regarding charge transfer within the molecule. The temperature dependence of the thermodynamic functions and their correlations were performed.

Synthesis procedure of 4-AminoPhthalhydrazide

In this experiment the chemiluminescent compound luminol, or 4-AminoPhthalhydrazide, will be synthesized from 4-nitrophthalic acid. It was performed by adding 10 g phthalimidehydrate in 20 ml water to a suspension of 4-nitrophthalimide (38.4 g′) of 4-nitrophthalimide in 250 ml water and refluxing for an hour. When this solution is acidified with acetic acid a pale yellow crystalline product is collected with suction on cooling. Purification was accomplished with solution in 3 L boiling 50% acetic acid, rapid filtration, followed by cooling and collection of pale yellow product. The melting point of 4-AminoPhthalhydrazide 299–300 °C. The calculated (found) % for $C_8H_7N_3O_2$: C, 54.24 (53.24); H, 3.98(3.95); N, 23.72 (22.71) and O, 18.06 (17.04). The first step of the synthesis in the simple formation of cyclic diamide, 4-nitrophthalhydrazide by reaction of 4-nitrophthalic acid with hydrazine.

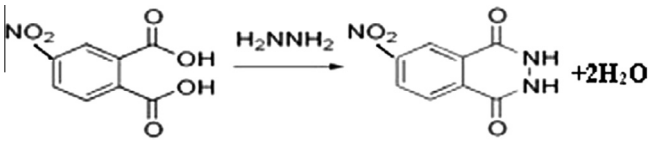

In the second step 4-nitrophthalhydrazide back to the large side-arm test tube. Add 6.5 ml of a 10% sodium hydroxide solution, and stir the mixture until the hydrazide dissolves. Add 4 g of sodium dithionite (sodium hydrosulfite). Using a pipet, add about 10 ml of water to wash the solid from the walls of the test tube. Heat the test tube with a micro burner until the solution boils. Stir the solution with a long glass rod. Maintain the boiling, with stirring, for 5 min. Add 2.6 ml of glacial acetic acid. Cool the test tube to room temperature. Stir the mixture during this cooling step. Finally, cool the solution in an ice bath. Collect the crystals of luminal by vacuum filtration using a Hirsch funnel.

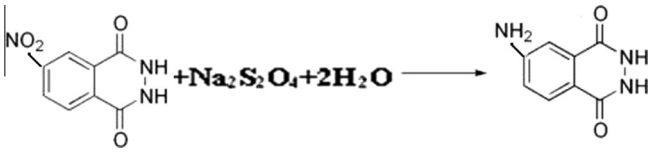

The reliability of the results of normal coordinate analysis depends on the availability of spectral data like frequencies. For a large number of molecules, this data may not be available. Spectral data of high precision can be obtained for the sample using the sophisticated spectroscopic equipments with the advent of powerful monochromatic laser source and photoelectric recording in both Raman and infrared instruments, quality spectral can be recorded in a short interval of time. All the chemical purchased from Lancaster chemical company, U.K. and used as such without any further purification. Fourier transform infrared (FTIR) spectrum of the title molecule is recorded in the range of 4000–400 cm^{-1} at a resolution of ±cm^{-1} using a BRUKER IFS 66V FTIR spectrophotometer equipped with a cooled MCT detector. Boxcar apodization was used for the 250 averaged interferograms collected for both the samples and background. The FT-Raman spectrum is recorded on a computer interfaced BRUKER IFS model interferometer, equipped with FRA 106 FT-Raman accessory in the 3500–50 cm^{-1} stokes region, using the 1064 nm line of Nd:YAG laser for excitation operating at 200 mW power. The reported wave numbers are believed to be accurate within ±1 cm^{-1}. The UV–visible absorption spectra of APH are examined in the range 200–500 nm using SHIMADZU UV-1650 PC, UV–vis recording spectrometer. The UV pattern is taken from 10^{-5} molar solution of APH, solved in ethanol.

Computational details

Density functional theory calculations are carried out for APH, Hartree–Fock (HF) and DFT calculations using GAUSSIAN 09W program package [15]. Initial geometry generated from the standard geometrical parameters was minimized without any constraint on the potential energy surface at Hartree–Fock level adopting the standard 6-311+G(d,p) basis set.

This geometry was then re-optimized again at DFT level employing the B3LYP keyword, which invokes Becke's three-parameter hybrid method [16] using the correlation function of Lee et al. [17], implemented with the same basis set for better

description of the bonding properties of amino group. All the parameters were allowed to relax and all the calculations converged to an optimized geometry which corresponds to a true minimum, as revealed by the lack of imaginary values in the wave number calculations. The Cartesian representation of the theoretical force constants have been computed at the fully optimized geometry. The multiple scaling of the force constants were performed according to SQM procedure [18] using selective scaling in the natural internal coordinate representation [19]. Transformation of force field, the subsequent normal coordinate analysis including the least square refinement of the scale factors and calculation of the total energy distribution (TED) were done on a PC with the MOLVIB program (version V7.0-G77) written by Sundius [20,21]. The systematic comparison of the results from DFT theory with results of experiments has shown that the method using B3LYP functional is the most promising in providing correct vibrational wave numbers. The calculated geometrical parameters were compared with X-ray diffraction result [22]. Normal coordinate analyses were carried out for the title compound to provide a complete assignment of fundamental frequencies. For this purpose, the full set of 77 standard internal coordinates (containing 23 redundancies) for APH was defined as given in Table 1. From these, a non-redundant set of local symmetry coordinates were constructed by suitable linear combinations of internal coordinates following the recommendations of Fogarasi et al. [19] is summarized in Table 2. The theoretically calculated force fields were transformed to this set of vibrational coordinates and used in all subsequent calculations.

Prediction of Raman intensities

The Raman activities (S_i) calculated with the GAUSSIAN 09W program are subsequently converted to relative Raman intensities

Table 2
Definition of local symmetry coordinates of 4-AminoPhthalhydrazide.

No. (i)	Type	Definition[a]
1–3	C H	R_1, R_2, R_3
4–11	CC	r_4, r_5, r_6, r_7, r_8, r_9, r_{10}, r_{11}
12	NN	S_{12}
13–15	NC	q_{13}, q_{14}, q_{15}
16, 17	NH	p_{16}, p_{17}
18, 19	CO	X_{18}, X_{19}
20	NH_2ss	$(Q_{20} + Q_{21})/\sqrt{2}$
21	NH_2ips	$(Q_{20} - Q_{21})/\sqrt{2}$
22	R_1trigd	$(\alpha_{22} - \alpha_{23} + \alpha_{24} - \alpha_{25} + \alpha_{26} - \alpha_{27})/\sqrt{6}$
23	R_1symd	$(-\alpha_{22} - \alpha_{23} + 2\alpha_{24} - \alpha_{25} - \alpha_{26} - 2\alpha_{27})/\sqrt{12}$
24	R_1asymd	$(\alpha_{22} - \alpha_{23} + \alpha_{25} - \alpha_{26})/\sqrt{2}$
25	R_2trigd	$(\alpha_{28} - \alpha_{29} + \alpha_{30} - \alpha_{31} + \alpha_{32} - \alpha_{33})/\sqrt{6}$
26	R_2symd	$(-\alpha_{28} - \alpha_{29} + 2\alpha_{30} - \alpha_{31} - \alpha_{32} - 2\alpha_{33})/\sqrt{12}$
27	R_2asymd	$(\alpha_{28} - \alpha_{29} + \alpha_{31} - \alpha_{32})/\sqrt{2}$
28–30	b C H	$(\beta_{34} - \beta_{35})/\sqrt{2}$, $(\beta_{36} - \beta_{37})/\sqrt{2}$, $(\beta_{38} - \beta_{39})/\sqrt{2}$
31	b NH	$b_{40} - b_{41}/\sqrt{2}$, $g_{42} - g_{43}/\sqrt{2}$
32	b NN	$g_{42} - g_{43}/\sqrt{2}$
33, 34	b CO	$(Z_{44} - Z_{45})/\sqrt{2}$, $(L_{46} - L_{47})/\sqrt{2}$
35, 36	b CN	$X_{48} - X_{49}/\sqrt{2}$, $M_{50} - M_{51}/\sqrt{2}$
37, 38	b NH	T_{52}, $(d_{53} - d_{54})/\sqrt{2}$
39–41	ω C H	ψ_{55}, ψ_{56}, ψ_{57}
42–44	ω NH	ρ_{58}, ρ_{59}, ρ_{60}
45, 46	ω CO	χ_{61}, χ_{62}
47	Ring trigd	$(\tau_{63} - \tau_{64} + \tau_{65} - \tau_{66} + \tau_{67} - \tau_{68})/\sqrt{6}$
48	Ring symd	$(\tau_{63} - \tau_{65} + \tau_{66} - \tau_{68})/\sqrt{2}$
49	Ring asymd	$(-\tau_{63} + 2\tau_{64} - \tau_{65} - \tau_{66} + 2\tau_{67} - \tau_{68})/\sqrt{12}$
50	Ring trigd	$(\tau_{69} - \tau_{70} + \tau_{71} - \tau_{72} + \tau_{73} - \tau_{74})/\sqrt{6}$
51	Ring symd	$(\tau_{69} - \tau_{71} + \tau_{72} - \tau_{73})/\sqrt{2}$
52	Ring asymd	$(-\tau_{69} + 2\tau_{70} - \tau_{71} - \tau_{72} + 2\tau_{73} - \tau_{74})/\sqrt{12}$
53	t C-NH_2	τ_{75}
54	Butterfly	$(\tau_{76} - \tau_{77})/\sqrt{2}$

[a] The internal coordinates used here are defined in Table 1.

Table 1
Definition of internal coordinates of 4-AminoPhthalhydrazide.

No. (i)	Symbol	Type	Definition[a]
Stretching			
1–3	R_i	C–H	C_3–H_{14}, C_5–H_{20}, C_6–H_{19}
4–11	r_i	C–C	C_1–C_2, C_2–C_3, C_3–C_4,C_4–C_5, C_5–C_6, C_6–C_1,C_1–C_7, C_2–C_{10}
12	S_i	N–N	N_8–N_9
13–15	q_i	N–C	N_8–C_7, N_9–C_{10}, N_{11}–C_4
16–17	P_i	N–H	N_8–H_{16}, N_9–H_{17}
18, 19	x_i	C–O	C_7–O_{18}, C_{10}–O_{15}
20, 21	Q_i	NH_2	N_{11}–H_{12}, N_{12}–H_{13}
In-plane bending			
22–27	α_i	Ring1	C_1–C_2–C_3, C_2–C_3–C_4, C_3–C_4–C_5, C_4–C_5–C_6, C_5–C_6–C_1, C_6–C_1–C_2
28–33	α_i	Ring2	C_7–N_8–N_9, N_8–N_9–C_{10}, N_9–C_{10}–C_2, C_{10}–C_2–C_1, C_2–C_1–C_7, C_1–C_7–N_8
34–39	β_i	C–C–H	C_1–C_6–H_{19}, C_5–C_6–H_{19}, C_6–C_5–H_{20}, C_4–C_5–H_{20}, C_2–C_3–H_{14}, C_4–C_3–H_{11}
40, 41	b_i	C–N–H	C_7–N_8–H_{17}, C_{10}–N_9–H_{16}
42, 43	g_i	N–N–H	N_9–N_8–H_{17}, N_8–N_9–H_{16}
44, 45	Z_i	C–C–O	C_1–C_7–O_{18}, C_2–C_{10}–O_{15}
46, 47	L_i	N–C–O	N_8–C_7–O_{18}, N_9–C_{10}–O_{15}
48, 49	X_i	C–C–N	C_3–C_4–N_{11}, C_5–C_4–N_{11}
50–51	M_i	C–N–H	C_4–N_{11}–H_{12}, C_4–N_{11}–H_{12}
52	T_i	H–N–H	H_{12}–N_{11}–H_{13}
53, 54	d_i	N–N–H	N_9–N_8–H_{17}, N_8–N_9–H_{16}
Out-of-plane bending			
55–57	ψ_i	C–H	H_{14}–C_3–C_2–C_4, H_{19}–C_6–C_5–C_1, H_{20}–C_5–C_6–C_4
58–60	ρ_i	H–N	H_{16}–N_9–C_{10}–N_8, H_{17}–N_8–N_9–C_7, C_4–N_{11}–H_{12}–H_{13}
61, 62	χ_i	C–O	O_{15}–C_{10}–N_9–C_2, O_{18}–C_7–N_8–C_1
Torsion			
63–68	τ_i	t Ring	C_1–C_2–C_3–C_4, C_2–C_3–C_4–C_5, C_3–C_4–C_5–C_6, C_4–C_5–C_6–C_1, C_5–C_6 –C_1–C_2, C_6–C_1–C_2–C_3
69–74	τ_i	t Ring	C_7–C_8–C_9–C_{10}, C_8–C_9–C_{10}–C_2, C_9–C_{10}–C_2–C_1, C_{10}–C_2–C_1–C_7, C_2–C_1–C_7–C_8, C_1–C_7–C_8–C_9
75	τ_i	t C-NH_2	C_4–N_{11}–H_{12}–H_{13}
76, 77	τ_i	Butterfly	C_6–C_1–C_2–C_{10}, C_7–C_1–C_2–C_3

[a] For numbering of atoms refer Fig. 1.

(I_i) using the following relationship derived from the basic theory of Raman scattering [23]

$$I_i = \frac{f(v_0 - v_i)^4 S_i}{v_i\left[1 - \exp\frac{-hcv_i}{kT}\right]}$$

where v_0 is the exciting frequency in cm^{-1}, v_i the vibrational wave number of the ith normal mode, h, c and k are the fundamental constants and f is a suitably chosen common normalization factor for all the peak intensities.

Results and discussion

Molecular geometry

The optimized molecular structure of APH along with numbering of atoms is shown in Fig. 1. The optimized structure parameters of APH obtained by DFT-B3LYP/6-311+G(d,p) and HF/6-311+G(d,p) levels are listed in Table 3. From the structural data given in Table 3, it is observed that the various bond lengths are found to be almost same at HF/6-311+G(d,p) level of theory, in general slightly over estimates bond lengths but it yields bond angles in excellent agreement with the HF method. The calculated geometric parameters can be used as foundation to calculate the other parameters for the compound. The optimized molecular structure of APH reveals that the N-heterocyclic rings of amino group are in planar. Inclusion of CH group and NH atoms known for its strong electron-withdrawing nature, in heterocyclic position, is expected to increase a contribution of the resonance structure, in which the electronic charge is concentrated at this site. This is the reason for the shortening of bond lengths N11–H12 = 0.994 Å and N11–H13 = 0.995 Å obtained by HF method. The same bond lengths calculated by DFT method is found to be 1.009 Å and 1.010 Å. The carbon atoms are bonded to the hydrogen atoms with an σ-bond in heterocyclic ring and the substitution of hydrogen atoms for hydrogen reduces the electron density at the ring carbon atom. In APH, the N–H bond lengths vary from 0.997 Å to 0.999 by HF method and from 1.013 to 1.014 B3LYP methods. The ring carbon atoms in substituted heterocyclic exert a larger attraction on the valence electron cloud of the hydrogen atom resulting in an increase in the C–H force constants and a decrease in the corresponding bond length. It is evident from the C–C bond lengths ranging from 1.375 Å to 1.489 Å by HF method and from 1.385 to 1.485 by B3LYP method in the heterocyclic rings of APH, whereas the C–H bond lengths in APH vary from 1.073 Å to1.076 Å and from 1.084 to 1.086 Å by HF and B3LYP methods, respectively. The heterocyclic rings appear to be a little distorted because of the NH_2 group substitution as seen from the bond angles C3–C4–C5 which are calculated as 118.96° and 118.76° respectively, by HF and B3LYP methods and they are smaller than typical hexagonal angle of 120°. The comparative graphs of bond lengths, bond angles and dihedral angles of APH for three sets are presented in Figs. 2–4 respectively. From the theoretical values, it is found that most of the optimized bond lengths are slightly larger than the experimental values, due to that the theoretical calculations belong to isolated molecules in solid phase and the experimental results belongs to molecules in solid state.

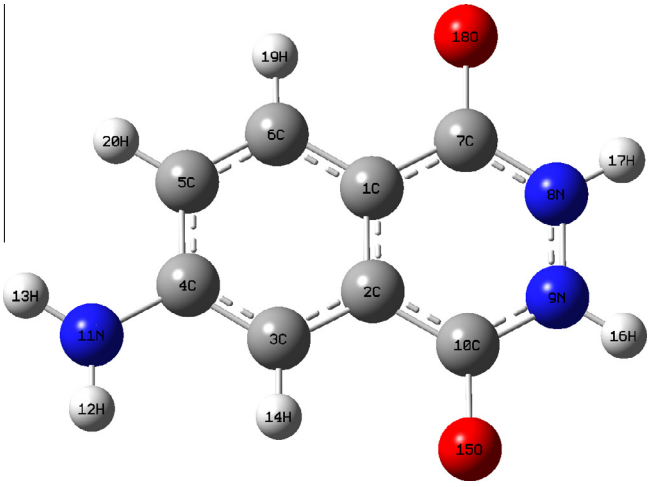

Fig. 1. Molecular structure of 4-AminoPhthalhydrazide.

First hyperpolarizability

The potential application of the title compound in the field of nonlinear optics demands, the investigation of its structural and bonding features contribution to the hyperpolarizability enhancement, by analyzing the vibrational modes using IR and Raman spectroscopy. Many organic molecules, containing conjugated π electrons are characterized by large values of molecular first hyper polarizabilities, were analyzed by means of vibration spectroscopy [24]. In most of the cases, even in the absence of inversion symmetry, the strongest band in the IR spectrum is weak in the Raman spectrum and vice versa. But the intramolecular charge from the donor to acceptor group through a π-bond conjugated path can induce large variations of both the molecular dipole moment and the molecular polarizability, making IR and Raman activity strong at the same time. The experimental spectroscopic behavior described above is well accounted for a calculations in π conjugated systems that predict exceptionally infrared intensities for the same normal modes. The first hyperpolarizability (β) of this novel molecular system is calculated using the *ab initio* quantum mechanical method, based on the finite-field approach. In the presence of an applied electric field, the energy of a system is a function of the electric field. The first hyperpolarizability is a third-rank tensor that can be described by a $3 \times 3 \times 3$ matrix. The 27 components of the 3D matrix can be reduced to 10 components due to the Kleinman symmetry [25]. The components of β are defined as the coefficients in the Taylor series expansion of the energy in the external electric field. When the electrical field is weak and homogeneous, this expansion becomes

$$E = E_0 - \sum_i \mu_i F^i - \frac{1}{2}\sum_{ij} \alpha_{ij} F^i F^j - \frac{1}{6}\sum_{ijk} \beta_{ijk} F^i F^j F^k - \frac{1}{24}\sum_{ijkl} v_{ijkl} F^i F^j F^k F^l$$

where E_0 is the energy of the unperturbed molecule; F^i is the field at the origin; and μ_i, α_{ij}, β_{ijk} and γ_{ijkl} and are the components of dipole moment, polarizability, the first hyperpolarizabilities and second hyperpolarizabilities, respectively. The calculated total dipole moment (μ) and mean first hyperpolarizability (β) of APH are 1.1437 Debye and 8.3541×10^{-30} esu, respectively, which is comparable with the reported values of similar derivatives. The large value of hyperpolarizibilities, β which is a measure of the non-linear optical activity of the molecular system, is associated with the intramolecular charge transfer, resulting from the electron cloud movement through π conjugated frame work from electron donor to electron acceptor groups. The physical properties of these conjugated molecules are governed by the high degree of electronic charge delocalization along the charge transfer axis and by the low band gaps. So we conclude that the title compound is an attractive object for future studies of nonlinear optical properties.

Table 3
Optimized geometrical parameters of 4-AminoPhthalhydrazide obtained by HF/6-31+G(d,p) and B3LYP/6-311G+(d,p) density functional theory calculations.

Bond length	Value (Å)		Exp[a]	Bond angle	Value (°)		Exp[a]
	HF/6-311+G(d,p)	B3LYP/6-311+G(d,p)			HF/6-311+G(d,p)	B3LYP/6-311+G(d,p)	
C1–C2	1.387	1.408	1.359	C2–C1–C6	118.96	118.78	120.3
C1–C6	1.391	1.403	1.383	C2–C1–C7	120.94	121.27	121.7
C1–C7	1.474	1.472		C6–C1–C7	120.12	119.91	119.8
C2–C3	1.382	1.393	1.415	C1–C2–C3	121.22	120.88	121.6
C2–C10	1.489	1.485		C1–C2–C10	119.81	120.41	
C3–C4	1.392	1.404	1.423	C3–C2–C10	118.93	118.67	
C3–H14	1.074	1.085	0.917	C2–C3–C4	119.82	120.21	116.4
C4–C5	1.402	1.415	1.391	C2–C3–H14	119.05	118.47	
C4–N11	1.379	1.381	1.347	C4–C3–H14	121.11	121.30	
C5–C6	1.375	1.385	1.364	C3–C4–C5	118.96	118.76	121.1
C5–H20	1.076	1.086	0.884	C3–C4–N11	120.66	120.74	122.5
C6–H19	1.073	1.084	0.920	C5–C4–N11	120.33	120.45	119.8
C7–N8	1.371	1.387		C4–C5–C6	120.72	120.77	119.6
C7–O18	1.201	1.229		C4–C5–H20	119.41	119.34	121.7
N8–N9	1.401	1.411		C6–C5–H20	119.85	119.88	
N8–H17	0.999	1.014	0.872	C1–C6–C5	120.34	120.56	
N9–C10	1.363	1.378	1.460	C1–C6–H19	118.92	118.47	120.3
N9–H16	0.997	1.013	1.405	C5–C6–H19	120.73	120.96	123.3
C10–O15	1.199	1.229		C1–C7–N8	116.00	115.41	
N11–H12	0.994	1.009	0.908	C1–C7–O18	124.04	125.00	
N11–H13	0.995	1.010	0.887	N8–C7–O18	119.95	119.57	
				C7–N8–N9	121.61	122.02	119.8
				C7–N8–H17	112.55	113.73	115.2
				N9–N8–H17	111.85	113.08	
				N8–N9–C10	122.47	122.95	

Dihedral angle	Value (°)		Exp[a]
	HF/6-311+G(d,p)	B3LYP/6-311+G(d,p)	
C6–C1–C2–C3	−0.7074	−0.733	
C6–C1–C2–C10	−179.01	−178.91	
C7–C1–C2–C3	−178.77	−178.84	
C7–C1–C2–C10	2.916	2.972	
C2–C1–C6–C5	0.5978	0.5812	
C2–C1–C6–H19	−179.40	−179.50	
C7–C1–C6–C5	178.68	178.72	
C7–C1–C6–H19	−1.314	−1.3642	
C2–C1–C7–N8	−7.242	−6.9752	
C2–C1–C7–O18	173.28	173.70	
C6–C1–C7–N8	174.71	174.93	
C6–C1–C7–O18	−4.757	−4.3905	
C1–C2–C3–C4	0.436	0.539	
C1–C2–C3–H14	−179.78	−179.63	
C10–C2–C3–C4	178.75	178.75	
C10–C2–C3–H14	−1.465	−1.4214	
C1–C2–C10–N9	−7.406	−6.485	
C1–C2–C10–O15	173.11	174.06	
C3–C2–C10–N9	174.24	175.29	
C3–C2–C10–O15	−5.230	−4.158	
C2–C3–C4–C5	−0.049	−0.182	
C2–C3–C4–N11	177.64	177.54	
H14–C3–C4–C5	−179.82	179.99	
H14–C3–C4–N11	−2.1264	−2.276	
C3–C4–C5–C6	−0.052	0.0336	

For numbering of atoms refer Fig. 1.
[a] Value taken from Ref. [22].

NMR spectral analysis

The isotropic chemical shifts are frequently used as an aid in identification of reactive organic as well as ionic species. It is recognized that accurate predictions of molecular geometries are essential for reliable calculations of magnetic properties. Therefore, full geometry optimization of APH were performed by using B3LYP/6-311+G(d,p) method. Then, Gauge-Including Atomic Orbital (GIAO) ^{1}H and ^{13}C chemical shift calculations of the compound has been made by same method. Application of the GIAO [26] approach to molecular systems was significantly improved by an efficient application of the method to the *ab initio* SCF calculations, using techniques borrowed from analytic derivative methodologies. GIAO procedure is somewhat superior since it exhibits a faster convergence of the calculated properties upon extension of the basis set used. Taking into account the computational cost and the effectiveness of calculation, the GIAO method seems to be preferable from many aspects at the present state of this subject. On the other hand, the density functional methodologies offer an effective alternative to the conventional correlated methods, due to their significantly lower computational cost. The molecular structure of APH is optimized by B3LYP method with 6-311+G(d,p). Then, gauge-including atomic orbital (GIAO) ^{13}C and ^{1}H chemical shift calculation of title compound is made by using B3LYP method. The ^{1}H and ^{13}C chemical shifts were measured in a less polar (CDCl3) solvent. The result in Table 4 shows that the range ^{13}C NMR chemical shift of the typical organic molecule usually is >100 ppm [27,28], the accuracy ensures

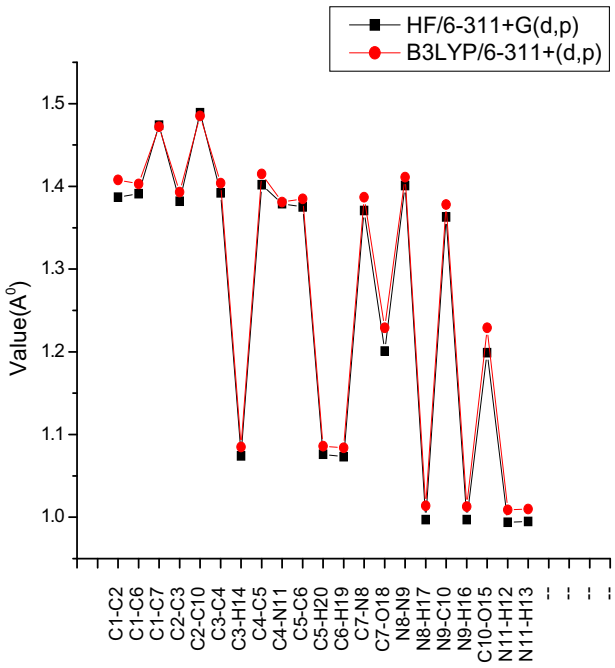

Fig. 2. Bond length differences between theoretical (HF and DFT) approaches.

reliable interpretation of spectroscopic parameters. It is true from the above literature value, in our present study, the title molecule also falls with the above literature data except with the carbon atoms (C4). In the present paper, the signal observed at 190.30 ppm in ^{13}C NMR spectrum is assigned to C10 carbon atom correlates with theoretically predicted value at 187.473 ppm. The signals for aromatic carbons were observed at 127.70–184.70 ppm in ^{13}C NMR spectrum for the title molecule, since those carbon atoms which belong to APH also exactly correlate with theoretically predicted value at 131.096–186.714 ppm. The signals of the aromatic proton were observed at 21.01–23.20 ppm. The calculated proton NMR chemical shifts show moderate agreement with the experimental values except with aliphatic proton H16, H17. The H atom is the smallest of all atoms and

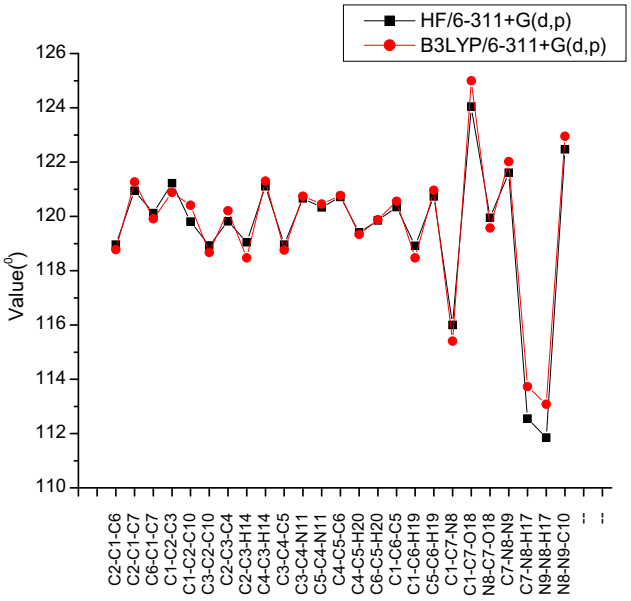

Fig. 3. Bond angle differences between theoretical (HF and DFT) approaches.

mostly localized on the periphery of molecules. Therefore their chemical shifts would be more susceptible to intermolecular interactions in the aqueous solution as compared to that for other heavier atoms. Another important aspect is that, hydrogen attached or nearby electron with drawing atom or group can decrease the shielding and moves the resonance of attached proton towards to a higher frequency. By contrast electron donating atom or group increases the shielding and moves the resonance towards to a lower frequency. In this study, the chemical shifts obtained and calculated for the hydrogen atoms of amino groups are high. All values are [29] due to shielding effect. It is true from above literature data in our present study the amino protons at N11 appears as singlet with two proton integral at 27.40–27.41 ppm shows good agreement with computed chemical shift values are shown in Table 4. The relationship between the experimental chemical shift and computed chemical shift GIAO/B3LYP/6-311+G(d,p) levels for ^{13}C are shown in Fig. 5.

HOMO–LUMO analysis

This electronic absorption correspond to the transition from the ground to the first excited state and is mainly described by one electron excitation from the highest occupied molecular orbital (HOMO) to the lowest unoccupied molecular orbital (LUMO) [30,31]. The HOMO is located over nitrogen and hydrogen group and the HOMO–LUMO transition implies an electron density transfer to the oxygen group from heterocyclic ring to nitrogen group. Moreover, these orbital's significantly overlap in their position for APH. The HOMO–LUMO energy gap of APH was calculated at B3LYP level, which reveals that the energy gap reflects the chemical activity of molecule. The LUMO as an electron acceptor (EA) represents the ability to obtain an electron (ED) and HOMO represents ability to donate an electron (ED). The ED groups to the efficient EA groups through π-conjugated path. The strong charge transfer interaction through π-conjugated bridge results in substantial ground state Donor–Acceptor (DA) mixing and the appearance of a charge transfer band in the electron absorption spectrum. The atomic orbital compositions of the frontier molecular orbital and few MOs are sketched in Fig. 6. The calculated self-consistent field (SCF) energy of APH is – 623.9537 a.u. The HOMO and LUMO energy gap explains the fact that eventual charge transfer interaction is taking place within the molecule.

Global and local reactivity descriptors

Based on density functional descriptors global chemical reactivity descriptors of molecules such as hardness, chemical potential, softness, electronegativity and electrophilicity index as well as local reactivity have been defined [32–36]. Pauling introduced the concept of electronegativity as the power of an atom in a molecule to attract electrons to it. Hardness (η), chemical potential (μ) and electronegativity (χ) and softness are defined follows.

$$\eta = 1/2(\partial 2E/\partial N2)V(r) = 1/2(\partial\mu/\partial N)V(r)$$

$$\mu = (\partial E/\partial N)V(r)$$

$$\chi = -\mu = -(\partial E/\partial N)V(r)$$

where E and $V(r)$ are electronic energy and external potential of an N-electron system respectively. Softness is a property of molecule that measures the extent of chemical reactivity. It is the reciprocal of hardness:

$$S = 1/\eta$$

Using Koopmans's theorem for closed-shell molecules, η, μ and χ can be defined as

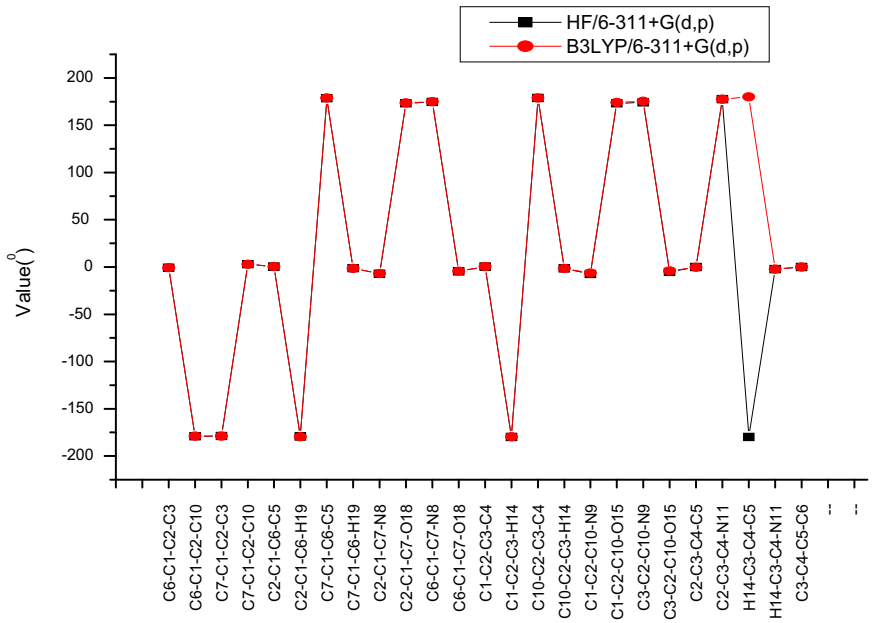

Fig. 4. Dihedral angle differences between theoretical (HF and DFT) approaches.

Table 4
Experimental and theoretical chemical shifts (^{13}C, ^{1}H) of 4-AminoPhthalhydrazide by B3LYP/6-311+G(d,p) method (ppm)].

Atom position	B3LYP	
	Expt	6-311+G(d,p
C1	65.90	114.474
C2	63.41	18.0531
C3	127.70	131.096
C4	153.56	155.568
C5	130.80	134.833
C6	131.01	134.19
C7	184.70	186.714
N8		110.43
N9		108.92
C10	190.30	187.473
N11		198.238
H12	27.40	30.606
H13	27.41	30.418
H14	21.01	24.056
O15		−211.405
H16	21.90	24.950
H17	22.03	25.037
O18		−197.021
H19	21.10	24.115
H20	23.20	25.459

$$\eta = (I - A)/2$$

$$\mu = -(I + A)/2$$

$$\chi = (I + A)/2$$

where A and I are the ionization potential and electron affinity of the molecules respectively. The ionization energy and electron affinity can be expressed through HOMO and LUMO orbital energies as $I = -E_{HOMO}$ and $A = -E_{LUMO}$. Electron affinity refers to the capability of a ligand to accept precisely one electron from a donor. However in many kinds of bonding viz covalent hydrogen bonding, partial charge transfer takes places. Recently Parr et al. [32] have defined a new descriptor to quantify the global electrophilic power of the molecule as electrophilicity index (ω), which defines a quantitative classification of the global electrophilic nature of a molecule Parr et al. [32] have proposed electrophilicity index (ω) as a measure of energy lowering due to maximal electron flow between donor and acceptor.

They defined electrophilicity index (ω) as follows

$$\omega = \mu^2/2\eta$$

The usefulness of this new reactivity quantity has been recently demonstrated in understanding the toxicity of various pollutants in terms of their reactivity and site selectivity [37–39]. The calculated value of electrophilicity index describes the biological activity of APH. All the calculated values of hardness, potential, softness and electrophilicity index are shown in Table 5.

UV-spectral analysis

Ultraviolet spectra analysis of APH have been investigated by TD-DFT/B3LYP/6-311++G(d,p) method in ethanol. The calculated visible absorption maxima of λ_{max} that are a function of the electron availability have been reported in Table 6. Calculations of molecular orbital geometry show that the visible absorption maxima of this molecule correspond to the electron transition between frontier orbitals such as translation from HOMO to LUMO. As can be seen from the UV–vis spectra absorption maxima values have been found to be 410, 348.8 and 312.08 nm. The λ_{max} is a function of substitution, the stronger the donor character of the substitution, the more the electrons pushed into the molecule, the larger the λ_{max}. These values may be slightly shifted by solvent effects. The role of substituents and of the solvent influences on the UV-spectrum. The visible band observed around 343.71 nm could be attributed to high delocalization of π-electrons. These bands may be due to electronic transition of $\pi \rightarrow \pi^*$. The calculated UV–vis spectrum is shown in Fig. 7.

Vibrational spectra

From the structural point of view the title compound is assumed to have C_1 point group symmetry. The 54 fundamental modes of vibrations arising for APH are classified into 37A' and 17A'' species. The A' and A'' species represent the in-plane and out-of-plane vibrations, respectively. For visual comparison, the observed and calculated FTIR and FT-Raman spectra of APH at HF

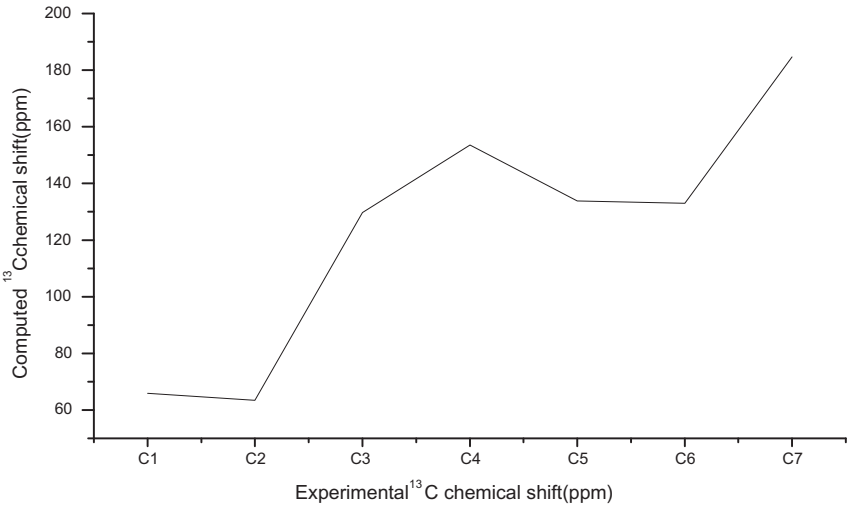

Fig. 5. Comparative graph of experimental chemical shift and computed chemical shift of ^{13}C of NMR.

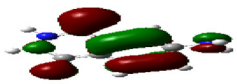

Homo-4 energy=-0.3389 a.u.

Lumo+4 energy= -0.0382 a.u.

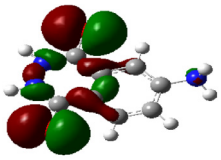

Homo-3 energy=-0.3359 a.u.

Lumo+3 energy= -0.0670 a.u.

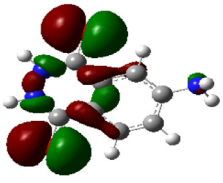

Homo-2 energy= -0.3351a.u.

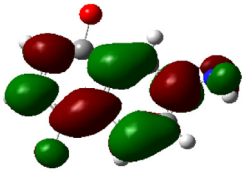

Lumo+2 energy= -0.0887 a.u.

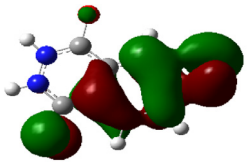

Homo-1 energy=-0.3243 a.u.

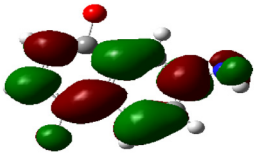

Lumo+1=-0.1707 a.u.

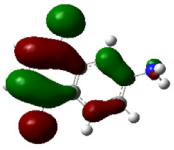

Homo energy=-0.2839a.u.

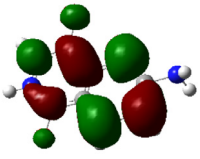

Lumo energy= -0.1781a.u.

Fig. 6. HOMO–LUMO plot of 4-AminoPhthalhydrazide.

Table 5
HOMO–LUMO energy gap and related molecular properties of 4-AminoPhthalhydrazide.

Molecular properties	B3LYP/6-311+G(d,p) (a.u.)
HOMO	−0.2839
LUMO	−0.1781
Energy gap	0.1058
Ionization potential (I)	0.2839
Electron affinity (A)	0.1781
Global softness (s)	18.9035
Global hardness (η)	0.0529
Chemical potential (μ)	−0.231
Global electrophilicity (ω)	0.5043

and DFT/B3LYP level using 6-311+G(d,p) basis set are shown in Figs. 8 and 9, respectively. The detailed vibrational assignment of fundamental modes of APH along with the calculated IR and Raman frequencies and normal mode descriptions (characterize by TED) are reported in Table 7. Comparison of frequencies calculated at HF and B3LYP with experimental values revels the overestimation of the calculated vibrational modes due to neglect of harmonicity in real system. Inclusion of electrons correlation in DFT values smaller in comparison with the HF frequencies data. The calculated frequencies are slightly higher than the observed value for the majority of normal modes. The major factor which is responsible for these discrepancies between the experimental and computed value is related to the fact that the experimental value is an anharmonic frequency while the calculated value is harmonic frequency. While an harmonicity is the main factor of the discrepancies in the case of vibrations related to the NH_2 and C═O bonds, for other vibrations most of the discrepancies come from the approximate nature of the used computational technique, and probably also from the lattice effects in the substance, studied as a solid. From the figure, it is found that the calculated (unscaled) frequencies by B3LYP with 6-311+G(d,p) basis sets are closer to the experimental frequencies than HF method with 6-311+G(d,p) basis set. This observation is supported by the literature report [24]. The standard deviation (SD) calculation made between experimental and computed frequencies (HF/DFT) for the APH is presented in Table 8. According to the SD, the computed frequency deviation decrease in going from HF/6-311+G(d,p) and B3LYP/6-311+G(d,p). The deviation ratio between HF/6-311+G(d,p) and B3LYP/6-31+G(d,p) is 2.60. It also proved that, the calculated frequencies by B3LYP/6-311+G(d,p) basis sets are closer to the experimental frequencies than HF method.

Table 6
The computed excitation energies, oscillator strength, electronic transition configuration wavelength of 4-AminoPhthalhydrazide using TD-DFT/B3LYP/6-311+G(d,p).

Excited state	EE (eV)	Oscillator strength f	Configuration	CI expansion coefficient	Wavelength (nm)
1	2.5419	0.0000	45 → 48	0.10436	487.76
			46 → 47	−0.67862	
			46 → 47	0.67862	
2	2.9139	0.0055	42 → 47	0.19440	425.50
			45 → 47	−0.41471	
			46 → 48	0.44417	
			42 → 47	−0.19440	
			45 → 48	0.19845	
3	3.1891	0.0000	42 → 48	0.13036	388.78
			45 → 47	0.34885	
			45 → 48	0.30215	
			46 → 48	0.47218	
			45 → 47	−0.34885	
			45 → 48	−0.30215	
			46 → 48	−0.47218	
4	3.3644	0.1788	42 → 48	0.16992	368.52
			43 → 47	−0.18248	
			43 → 48	0.14568	
			44 → 47	−0.13277	
			45 → 47	−0.40187	
			45 → 48	0.43448	
			43 → 48	−0.14568	
			44 → 46	0.13277	
			45 → 48	−0.43448	
5	3.4654	0.0000	43 → 47	0.18827	357.78
			43 → 48	0.18081	
			44 → 47	−0.51423	
			44 → 48	−0.36935	
			44 → 47	0.51423	
			44 → 48	0.36935	
6	3.5005	0.0345	42 → 47	0.10409	354.19
			43 → 47	−0.50595	
			43 → 48	0.27885	
			43 → 47	0.50595	
			43 → 48	−0.27885	
			44 → 47	0.19475	
			44 → 48	−0.19981	

C–H vibrations

The hetero aromatic structure shows the presence of C–H stretching vibration in the region 3100–3000 cm^{-1} which is the characteristic region for the ready identification of C–H stretching vibration [41]. In this region, the bands are not affected appreciably by the nature of substituents. The C–H stretching mode usually appears with strong Raman intensity and is highly polarized. In the FT-IR spectrum of APH, the weak bands at 3050, and 3000 cm^{-1} are assigned to C–H stretching vibrations of hetro cyclic group. The counter part of the FT-Raman spectrum at 3015 cm^{-1} is attributed to C–H stretching vibration. The theoretically computed wavenumber by B3LYP method falls in the range at 3052–3001 cm^{-1} are assigned to C–H stretching vibration as shown in Table 7. The TED corresponding to this vibration is a pure mode, and contributing of 97%. The C–H in-plane bending frequencies appear in the range 1000–1300 cm^{-1} and are very useful for characterization purpose [42]. For our title molecule, the C–H in-plane bending vibrations appear as a weak to weak bands in FT-IR spectrum at 1198 and 1082 cm^{-1} and 1200 and 1196 cm^{-1} as a very weak to very weak band in FT-Raman spectrum shows good agreement with computed wavenumber by B3LYP/6-311+G(d,p) method at 1202–1084 cm^{-1}. The TED confirms these vibrations are mixed mode as it is evident from Table 7 almost contributing 40%. The C–H out-of-plane bending vibrations are strongly coupled vibrations and occur in the region 1000–750 cm^{-1} [43]. The

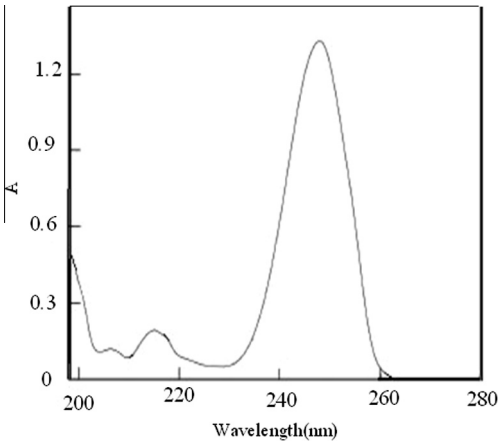

Fig. 7. UV spectrum of 4-AminoPhthalhydrazide.

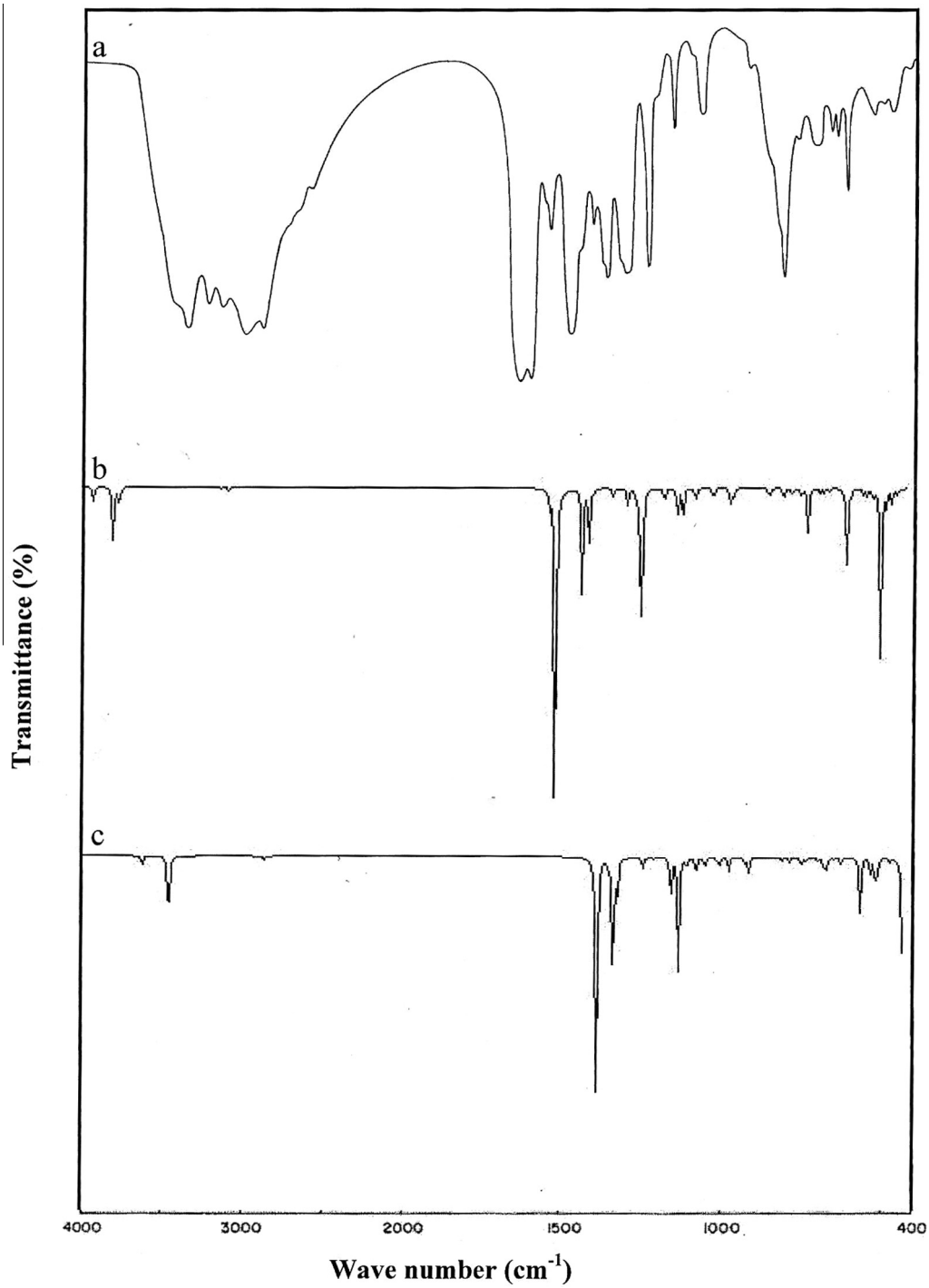

Fig. 8. Comparison of observed and calculated IR spectra of 4-AminoPhthalhydrazide (a) observed in solid phase, (b) calculated with B3LYP/6-311+G(d,p) and calculated with HF/6-311+G(d,p).

aromatic C–H out-of-plane bending vibration of APH are assigned as medium strong band observed at 718 cm^{-1} in FT-Raman and 735 and 729 cm^{-1} as a medium strong to very weak bands in FT-IR spectrum are well correlated with B3LYP/6-311+G(d,p) method at 738–719 cm^{-1} with TED contribution of 30%.

C═O vibrations

The structural unit of C═O has an excellent group frequency, which is described as a stretching vibration. Since the C═O group is a terminal group, only the carbon is involved in a second chemical bond this reduces the number of force constants determining the spectral position of the vibration. The C═O stretching vibration usually appears in a frequency range that relatively free of other vibrations. For example, in many carbonyl compounds the double bond of the C═O has a force constant different from those of such structural units such as C═C, C–C, C–H etc., only structural units of C═C have force constants of magnitudes similar to that of the C═O group. The C═C vibration could interact with C═O if it was the same species, but generally it is not. Almost all carbonyl compounds have a very intense and narrow peak in the range of 1800–1600 cm^{-1} [44,45] or in other words the carbonyl

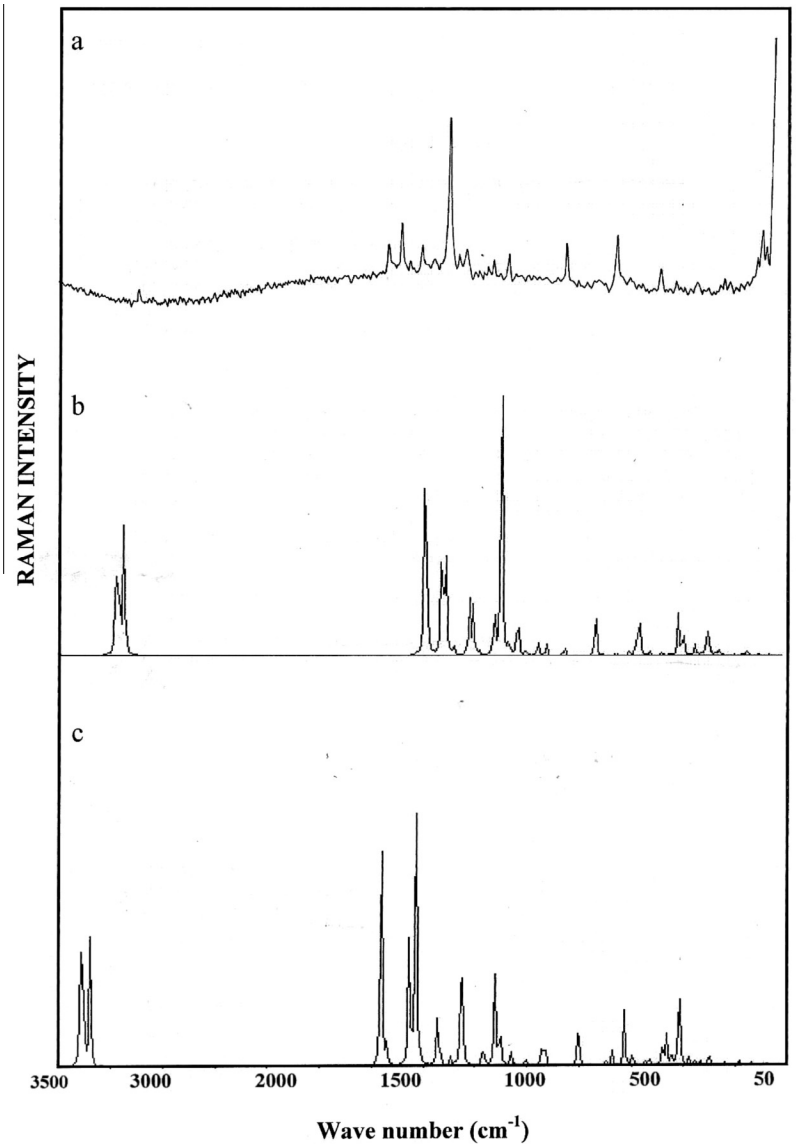

Fig. 9. Comparison of observed and calculated Raman spectra of 4-AminoPhthalhydrazide (a) observed in solid phase, (b) calculated with B3LYP/6-311+G(d,p) and calculated with HF/6-311+G(d,p).

stretching frequency has been most extensively studied by infrared spectroscopy [46]. The multiple bonded group is highly polar and therefore gives rise to an intense infrared absorption band in the region 1700–1800 cm^{-1}. The carbon–oxygen double bond is formed by Pπ–Pπ bonding between carbon and oxygen. Because of the different electro negativities of the carbon and oxygen atoms, the bonding electrons are not equally distributed between the two atoms. The following two resonance forms contribute to the bonding of the carbonyl group >C O←→C^{+}–O^{-}·. The lone pair of electrons on oxygen also determines nature of the carbonyl group [47]. In our present study, we can expect two C=O stretching vibration (i.e. C7=O18 and C10=O15), the conjugation of C10=O15 bond C7=O18 may increase its single bond character resulting in lowered values of carbonyl stretching wave numbers. The computed wave number by B3LYP/6-311+G(d,p) method at 1695 cm^{-1} is assigned to C10=O15 stretching vibrations. The strong band in FT-Raman at 1693 cm^{-1} is assigned to C10=C15 stretching mode. While in the case of C7=O18 stretching mode, the shoulder band in FT-IR spectrum at 1672 cm^{-1} are in moderate agreement with computed wave number at 1674 cm^{-1}. The lowering of wave number between the recorded as well as computed for C7=O18 stretch may be due to formation of intramolecular hydrogen bonding with adjacent CH moiety.

N–H vibrations

The hetero aromatic molecule containing an N–H group shows its stretching absorption in the region 3500–3220 cm^{-1}. This is usual range of appearance for NH_2 vibrations. The position of absorption in this region depends upon the degree of hydrogen bonding, and hence upon the physical state of the sample or the polarity of the solvent [48]. The vibrational bands due to the N–H stretching are sharper and weaker than those of C–O stretching vibrations by virtue of which they can be easily identified [49]. The N–H stretching fundamental of piperidine was observed in the vapor phase at 3364 cm^{-1}. Gulluoglu et al. [50,51] observed in the liquid phase at 3340 cm^{-1} for the N–H stretching of the piperidine. In our present study the very weak band observed in FT Raman spectrum at 3195 cm^{-1} and broad band in FT-IR spectrum at 3245 and 3194 cm^{-1} is assigned to N–H stretching vibration.

Table 7
The observed FT IR, FT-Raman and calculated (unscaled and scaled) frequencies (cm^{-1}), IR intensity (km mol^{-1}), Raman activity(A^0 amu-1). and force constant (m dyne A^0) and probable assignments(Characterized by TED) of 4-AminoPhthalhydrazide using B3LYP/6-311+G(d,p) and HF/6-311+G(d,p) calculations.

Symmetry species C_1	Observed frequencies (cm^{-1})		Calculated frequencies (cm^{-1}) (unscaled)		Scaling frequency (cm^{-1})		Force constant (mDyne/A)		IR intensity (kM/mol)		Raman activity (A^4/amu)		Assignment (% TED)
	FT7-IR	FT-RAMAN	HF	B3LYP	HF	B3LYP	HF	B3LYP	HF	B3LYP	HF	B3LYP	
A′	3352ms	–	3936	3714	3399	3354	10.052	8.9572	34.4492	29.1020	51.4689	63.8942	NH_2ass(99)
A′	3270ms	3272vw	3848	3598	3301	3271	9.4071	7.9904	91.4206	54.4516	112.400	317.400	NH_2ss(98)
A′	3245ms	–	3845	3596	3288	3244	9.3941	8.2166	69.3341	70.8244	91.8614	136.130	ν NH(96)
A′	3194w	3195vw	3820	3591	3220	3195	9.0184	8.1924	61.4561	71.5549	180.519	152.274	νNH(97)
A′	3050w	–	3394	3219	3090	3052	7.4329	6.6759	1.8532	2.4603	87.0880	100.587	νCH(93)
A′	–	3015w	3382	3204	3068	3014	7.3680	6.5985	3.3087	4.6828	51.0702	61.0710	νCH(94)
A′	3000w	–	3350	3182	3044	3001	7.2184	6.5022	12.6096	12.8585	97.2062	117.774	νCH(95)
A′	–	1693s	1952	1749	1721	1695	20.850	16.761	40.3830	27.4836	96.9603	140.589	$\nu C_{10}{=}O_{15}(52) + \nu C_7{=}O_{18}(35)$
A′	1672vs	–	1925	1734	1710	1674	20.013	15.296	1038.22	728.989	11.1084	12.0205	νC═O(66)
A′	–	1610s	1815	1669	1680	1611	2.4964	2.5478	277.74	400.755	55.1328	72.821	νCC(65), NH_2siss(33)
A′	1550ms	1550ms	1786	1650	1590	1553	7.2776	4.3733	173.891	122.226	146.688	76.425	NH_2siss(64), νC═O(31)
A′	1492s	–	1763	1610	1534	1494	13.452	11.117	13.9598	1.8244	5.3600	5.9784	νCC(60), νC═O(28)
A′	–	1488vs	1677	1537	1520	1490	3.2972	4.5510	25.7765	31.0339	25.2976	33.3893	νCC(92)
A′	1430s	–	1666	1518	1507	1431	4.0608	2.7173	2.7410	1.6812	2.3909	27.635	νCC(91)
A′	–	1410s	1615	1495	1488	1411	4.8396	3.8751	41.7697	6.8890	3.2794	2.1319	νCC(90)
A′	1382ms	–	1569	1453	1440	1384	3.2983	1.9633	143.211	125.504	30.7818	27.7756	νCC(51), νCN(23), bNH(19)
A′	–	1352ms	1558	1399	1399	1355	3.4802	8.0207	384.315	9.7534	39.9099	2.5137	νCC(52), νCN(30), bNH(17)
A′	–	1324w	1459	1354	1370	1326	2.7202	5.4908	46.741	290.340	9.4974	140.366	νCC(46), νCN(35), bCH(16)
A′	1301ms	–	1401	1338	1322	1305	4.7285	2.4526	79.773	32.6167	43.6925	8.5424	νCN(48), νNN(39), bCH(12)
A′	–	1291w	1378	1321	1312	1294	2.2849	3.7188	98.3102	52.4394	15.4910	22.9486	νCN(42), bNH(31), bCH(26)
A′	–	1273vw	1356	1317	1301	1277	2.9335	1.5582	2.1129	33.8240	0.8881	2.8489	νCN(67), bNH(33)
A′	–	1250ms	1322	1301	1270	1254	2.3498	1.9457	32.3403	27.0784	6.8650	7.6373	νNN(51), bCH(32), R_1asymd(13)
A′	1231w	–	1301	1278	1255	1233	1.3756	1.0354	37.6325	38.9137	3.4563	5.8072	bNH(49), bCH(33), R_1symd(17)
A′	–	1212w	1231	1221	1225	1214	2.3978	1.6275	36.4015	16.9881	3.1451	1.4208	bNH(48), bCH(32), R_1trigd(15)
A′	–	1200vw	1210	1180	1239	1202	1.4310	1.8330	5.5271	32.8545	2.7850	3.0296	bCH (47), NH_2rock(38), νCN(12)
A′	1198w	1196vw	1213	1199	1207	1197	2.1246	1.2839	36.2891	14.1331	9.6887	1.0408	bCH(46), R_1asymd(31), νCN(18)
A′	1082w	–	1113	991	1110	1084	0.9841	0.7650	0.6080	1.0290	0.3153	0.1706	bCH(45), R_1symd(30), νCN(22)
A′	–	1064w	1006	937	1100	1067	1.2751	1.9805	8.9294	9.1837	10.9773	20.6688	NH_2rock(49), R_1trigd(31), ωNH(18)
A′	–	1035vw	998	904	1070	1038	1.3957	0.7185	19.8925	14.3108	8.3671	0.1496	R_1asymd(45), bCO (32), ωNH(19)
A′	–	1010vw	946	850	1050	1013	0.8417	0.6717	30.5459	23.5194	0.6174	0.6773	R_1symd(47), ωNH(29), bCO(11)
A′	980w	–	909	829	1010	985	2.1917	1.9514	17.8447	13.6639	0.4078	0.5720	R_1trigd(44), ωNH(32), bCO(21)
A′	–	873w	868	776	899	877	2.1683	1.8759	26.0512	8.6864	2.2053	1.6320	R_2asymd(60), NH_2wag(32)
A′	862vs	–	839	747	880	864	3.1974	2.5785	115.541	56.0054	5.0192	5.0856	NH_2wag(65), bCO(32)
A′	–	821s	784	730	856	822	1.9269	1.9104	10.5929	4.9374	18.8803	20.9881	R_2symd(69), ωCH(28)
A′	790ms	–	766	711	810	794	1.1983	1.2136	16.0067	4.7622	1.0073	1.2335	R_2trigd(62), ωCH(29)
A′	–	772s	743	678	790	773	1.1804	0.9684	7.0684	20.3089	2.9791	1.8906	ωNH(51), R_1asymd(31), ωCH(13)
A′	761w	–	678	621	777	764	1.3025	1.1582	11.4700	1.6671	1.1820	1.4933	ωNH(49), R_1symd(32), ωCH(14)
A″	753vw	–	664	590	763	755	0.5072	0.3997	200.301	150.540	1.7199	0.5374	bCO(55), R_1trigd(28), ωCH(17)
A″	–	749w	598	544	759	749	0.8064	0.6287	16.9937	38.7213	5.3193	19.0146	bCO(60), R_2asymd(38)
A″	735ms	–	582	527	748	738	0.8124	0.6568	19.4920	34.2921	10.8988	3.3225	ωCH(62), R_2symd(28)
A″	729vw	–	555	519	741	730	0.3599	0.3155	37.2770	51.0549	4.9549	7.3723	ωCH(63), R_2trigd(33)
A″	–	718ms	520	463	723	719	0.2482	0.5885	435.88	9.2342	21.3462	4.9201	ωCH(64), tR_1asymd(35)
A″	–	552w	495	437	600	557	0.6009	0.3817	44.4156	4.6969	0.4052	1.5534	tR_1asymd(72)
A″	540w	–	472	409	589	544	0.4085	0.2595	37.9667	50.3506	2.2894	4.0659	tR_1symd(71)
A″	501ms	–	445	404	530	505	0.4690	0.1302	24.7558	385.067	1.5754	11.9521	tR_1trigd(69)
A″	491vw	491w	418	386	521	495	0.5452	0.3722	5.0019	2.3595	1.4269	1.6556	tR_2asymd(74)
A″	428w	428vw	377	364	500	432	0.6230	0.0860	10.9623	25.8499	2.8685	0.9397	tR_2symd(70), ωCO(28)
A″	–	400ms	338	349	489	402	0.0702	0.5172	20.1637	6.4530	0.4209	3.3123	bCN(52), tR_1symd(30), ωCO(12)
A″	–	392vw	303	279	432	395	0.2606	0.2251	1.5635	1.6309	0.8944	0.6703	tR_2trigd(64)

(*continued on next page*)

Table 7 (*continued*)

Symmetry species C_1	Observed frequencies (cm^{-1})		Calculated frequencies (cm^{-1}) (unscaled)		Scaling frequency (cm^{-1})		Force constant (mDyne/A)		IR intensity (kM/mol)		Raman activity (A^4/amu)		Assignment (% TED)
	FT7-IR	FT-RAMAN	HF	B3LYP	HF	B3LYP	HF	B3LYP	HF	B3LYP	HF	B3LYP	
A″	–	300w	234	235	378	303	0.1980	0.1866	1.6991	6.2309	1.3520	0.9149	ωCO(51), tR$_2$trigd(32), ωCN(15)
A″	–	285vw	221	215	320	289	0.1322	0.1656	1.005	2.44162	0.4967	1.7243	ωCO(66)
A″	–	271vw	166	157	298	274	0.0837	0.0732	0.9114	1.5780	0.7975	0.8168	ωCN(72)
A″	–	198w	113	109	234	197	0.0511	0.0515	8.5254	7.0904	0.4494	0.5338	NH$_2$twist(52)
A″	–	175w	93	91	211	177	0.0269	0.0265	6.1292	6.8361	0.4963	0.5088	Butterfly(61)

Abbreviations: ν – stretching; b – in-plane bending; ω – out-of-plane bending; asymd – asymmetric; symd – symmetric; t – torsion; trig – trigonal; w – weak; vw – very weak; vs – very strong; s – strong; ms – medium strong; ss – symmetric stretching; ass – asymmetric stretching; ips – in-plane stretching; ops – out-of-plane stretching; sb – symmetric bending; ipr – in-plane rocking; opr – out-of-plane rocking; opb – out-of-plane bending.

The theoretically computed wave number by B3LYP/6-311+G(d,p) method at 3244–3195 cm^{-1} is attributed to N–H stretching vibration. The TED also confirms that this vibration is a pure mode of contributing to 96%. The in-plane and out-of-plane bending vibration of N–H group are also supported by the literature [52].

NH_2 Vibrations

The title molecule APH under consideration possesses NH_2 group in the fourth position of the ring. The NH_2 group gives rise to six internal modes of vibrations viz., the symmetric stretching, the anti symmetric stretching, the symmetric deformation or the scissoring, the rocking, the wagging and torsional modes [53]. The NH_2 group has two NH stretching vibrations, one begging asymmetric and the other symmetric. The frequency of asymmetric vibration is higher than that of symmetric one. In APH the medium strong bands observed at 3352 and 3270 in the FT-IR are assigned to asymmetric and symmetric stretching vibration respectively. In the FT-Raman the very weak band at 3272 cm^{-1} is assigned to NH_2 symmetric stretching mode [54]. Based on the above conclusion, the theoretically scaled down wave number at 3354 and 3271 cm^{-1} B3LYP/6-311+G(d,p) method are assigned to NH_2 asymmetric and symmetric stretching vibrations respectively. In addition the NH_2 group has scissoring, rocking, wagging and torsion modes. The deformation vibration observed in the FT-Raman spectrum as a medium strong band at 1550 cm^{-1} is assigned to NH_2 scissoring vibration. The theoretically scaled down values at 1553–1611 cm^{-1} by B3LYP/6-311+G(d,p) methods respectively assigned to NH_2 scissoring vibration. The scaled down wave number by B3LYP/6-311+G(d,p) method at 1067 cm^{-1} is assigned to NH_2 rocking vibration and this vibration is far below the recorded spectral range. The frequency in the FR-IR spectrum at 862 cm^{-1} assigned to NH_2 wagging mode correlates with the frequencies 864 cm^{-1} computed by the B3LYP/6-311+G(d,p) methods respectively [55]. The NH_2 twisting vibration computed by B3LYP/6-311+G(d,p) method at 197 cm^{-1} shows good agreement with the recorded FT-Raman frequency of 175 cm^{-1}.

Ring vibrations

Most of the ring vibrational modes are affected by the substitutions in the ring of the title molecule. The characteristic ring stretching vibrations are assigned in the region 1650–1300 cm^{-1} [56]. The presence of conjugate substituent such as C–C, C–N, C═O or the presence of heavy element causes a doublet formation. Therefore, the C–C stretching vibrations of APH are found at 1610, 1488, 1410, 1352, 1324 cm^{-1} in Raman and 1492, 1430, 1382 cm^{-1} in FTIR spectrum. The theoretically computed values for C–C vibrational modes by B3LYP/6-311+G(d,p) method (1611–1326) gives excellent agreement with experimental data. The identification of C–N stretching frequencies is a rather difficult task, since the mixing of vibrations is possible in this region. The C–N stretching vibration is usually lies in the region 1400–1200 cm^{-1}. The C–N stretching is observed medium strong at

Table 8
Standard deviation of frequencies by HF/6-311+G(d,p) and (B3LYP)/6-311+G(d,p) basis sets.

Basic set levels	Total values	Average	Standard deviation	Deviation ratio
Experimental value	39,019	1500.73	–	–
HF/6-311+(d,p)	70,826	1311.59	99.12	2.60
B3LYP/6-31+(d,p)	65,652	1215.77	93.24	

Table 9
Thermodynamic properties of 4-AminoPhthalhydrazide determined at different temperatures with B3LYP/6-311+G(d,p) level.

T (K)	S (J/mol K)	C_p (J/mol K)	$\Delta H0 \rightarrow T$ (kJ/mol)
100.00	288.02	71.28	4.75
200.00	355.75	131.32	14.87
298.15	418.63	186.14	30.51
300.00	419.78	187.10	30.85
400.00	480.36	234.88	52.02
500.00	537.12	273.85	77.53
600.00	589.89	304.83	106.53
700.00	638.81	329.51	138.29
800.00	684.15	349.45	172.27
900.00	726.29	365.86	208.06
1000.00	765.57	379.56	245.35

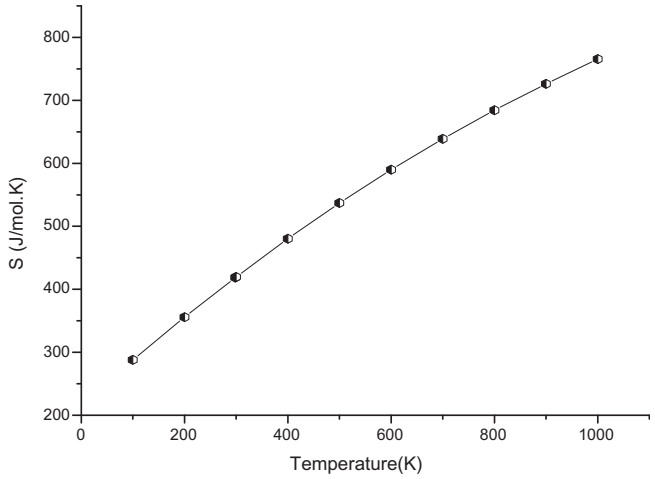

Fig. 10. The effect of temperature on entropy (S) of 4-AminoPhthalhydrazide.

1301 cm^{-1} and is mixed with C–O in-plane bending vibration. This frequency is also at the lower end of the expected range which may be also due to the interaction of C–C vibration, whose frequency extends up to this value. In this study, the bands observed at FT-IR 1301 cm^{-1} and in FT-Raman 1291, 1273 cm^{-1} of APH have been designated to C–N stretching vibrations. Also, in the present study, the bands ascribed at 980, 790 cm^{-1} in the FTIR and bands found at 1035, 1010, 873, 821 cm^{-1} in the Raman for the title molecule have been designated to ring in-plane bending modes by careful consideration of their quantitative descriptions. The ring out-of-plane bending modes of APH are also listed in Table 7. The reductions in the frequencies of these modes are due to the change in force constant and the vibrations of the functional groups present in the molecule. A part from these bands discussed for the title molecule there are some more absorption peaks in the observed spectra. These modes may be due to the lattice vibrations in the molecule. The lattice vibrations usually appear in the low frequency region. The low wave number hydrogen bonds expected in this region are usually weak. It is very difficult to specify exactly the appearance of any mode in this region. Some absorption peaks lying in between 400 and 150 cm^{-1} observed in Raman spectra, which are attributed to the combinations of translational and librational motions of APH.

Temperature dependence of thermodynamic properties

The temperature dependence of the thermodynamic properties heat capacity at constant pressure (C_p), entropy (S) and enthalpy change ($\Delta H0 \rightarrow T$) for APH were also determined by B3LYP/6-311++G(d,p) method and listed in Table 9. The Figs. 10–12 depicts

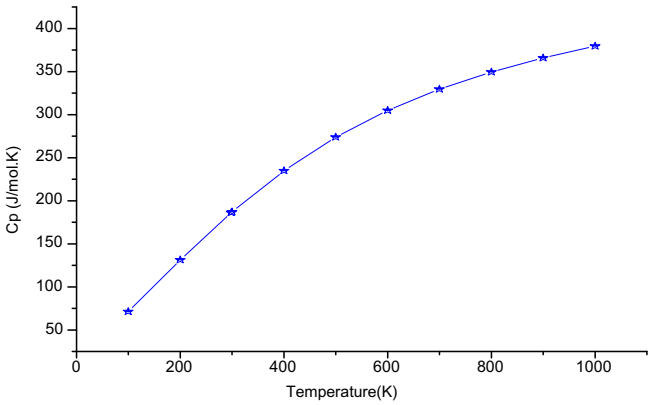

Fig. 11. The effect of temperature on heat capacity (C_p) of 4-AminoPhthalhydrazide.

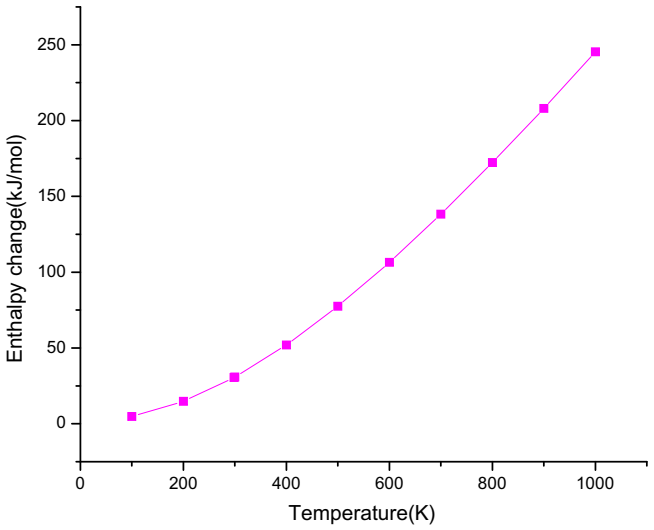

Fig. 12. The effect of temperature on enthalpy change ($\Delta H0 \rightarrow T$) of 4-AminoPhthalhydrazide.

the correlation of entropy (S), heat capacity at constant pressure (C_p) and enthalpy change ($\Delta H0 \rightarrow T$) with temperature along with the correlation equations. From Table 9, one can find that the entropies, heat capacities, and enthalpy changes are increasing with temperature ranging from 100 to 1000 K due to the fact that the molecular vibrational intensities increase with temperature [57]. These observed relations of the thermodynamic functions vs. temperatures were fitted by quadratic formulas, and the corresponding fitting regression factors (R2) are all not less than 0.9995. The corresponding fitting equations for APH are

$$S = 217.0465 + 0.5\ T - 1.3609 \times 10^{-4}\ T^2$$

$$C_p = 21.6851 + 0.3858\ T - 1.5329 \times 10^{-4}\ T^2$$

$$\Delta H = -4.1855 + 0.0587\ T + 1.1077 \times 10^{-4}\ T^2$$

Conclusion

In this present investigation molecular structure, vibrational frequencies, HOMO, LUMO, and polarizability analysis of APH have been studied using *ab initio* HF and DFT (B3LYP/6-311+G(d,p)) calculation. The NMR (^1H and ^{13}C) spectral studies are carried out at first time. Any discrepancy noted between the observed

and calculated frequencies may be due to the fact that the calculations have been actually done on a single molecule in the solid state contrary to the experimental values recorded in the presence of inter-molecular interactions. On the basis of the agreement between the calculated and observed results, assignments of fundamental vibrational modes of APH were examined and some assignments are proposed. This study demonstrates that scaled DFT/B3LYP calculations are powerful approach for understanding the vibrational spectra of medium sized organic compound. The UV spectrum was measured in ethanol solution. Temperature dependence of the thermodynamic properties heat capacity at constant pressure (C_p), entropy (S) and enthalpy change ($\Delta H0 \rightarrow T$) for APH were also determined by B3LYP/6-311+G(d,p) method. The theoretically constructed FT-IR and FT-Raman spectrum shows good correlation with experimentally observed FT-IR and FT-Raman spectrum.

References

[1] K.S. Markley, Fatty Acids, Their Chemistry Properties and Uses, Interscience Publishers, New York, 1964. pp. 1604–1608.
[2] E.A. Yousef, M.E. Zaki, M.G. Megahed, Heterocycl. Commun. 9 (2003) 293–298.
[3] D.L. Trepanier, E.R. Wagner, G. Harris, A.D. Rudzik, J. Med. Chem. 9 (1996) 881–885.
[4] K.K. Bedia, O. Elcin, U. Seda, K. Fatma, S. Nathaly, R. Sevim, A. Dimoglo, Eur. J. Med. Chem. 41 (2006) 1253–1261.
[5] H. Yin, J. Cui, Y. Qiao, Polyhedron 27 (2008) 2157–2166.
[6] G.M. Sheldrick, Acta Crystallogr. A 64 (2008) 112–122.
[7] Z.L. Xia, X. Hu, Bioorg. Med. Chem. 15 (2007). 3374–3374.
[8] K.K. Vijayaraj, B. Narayana, B.V. Ashalatha, N. Suchetha kumara, B.K. Sarojini, Eur. J. Med. Chem. 42 (2007) 425–429.
[9] A.H. Abadi, A.A.H. Eissa, G.S. Hassan, Chem. Pharm. Bull. 51–7 (2003) 838–844.
[10] C.G. Bonde, N.J. Gaikwad, Bioorg. Med. Chem. 12 (2004) 2151–2161.
[11] S.V. Bhandari, A.A. Patil, V. Sarkate, S.G. Gore, K.G. Bothra, Bioorg. Med. Chem. 17 (2009) 390–400.
[12] K. Sugano, H. Hamada, M. Machida, H. Ushio, J. Biomol. Screen. 6 (2001) 189–196.
[13] J.R. Duric, S.F. Bush, E.E. Mercer, J. Chem. Phys. 44 (1967) 4238.
[14] V. Krishnakumar, K. Parusuraman, A. Natarajan, Indian J. Pure Appl. Phys. 56 (1998) 171.
[15] Gaussian 09 Program, Gaussian Inc., Wallingford CT, 2009.
[16] A.D. Becke, J. Chem. Phys. 98 (1993) 5648–5652.
[17] C. Lee, W. Yang, R.G. Parr, Phys. Rev. B 37 (1988) 785–789.
[18] P. Pulay, G. Fogarasi, G. Pongor, J.E. Boggs, A. Vargha, J. Am. Chem. Soc. 105 (1983) 7037–7047.
[19] G. Fogarasi, P. Pulay, in: J.R. Durig (Ed.), Vibrational Spectra and Structure, vol. 14, Elsevier, Amsterdam, 1985, p. 125 (Chapter 3).
[20] T. Sundius, Vib. Spectrosc. 29 (2002) 89–95.
[21] MOLVIB (V.7.0): Calculation of Harmonic Force Fields and Vibrational Modes of Molecules, QCPE Program No. 807, 2002.
[22] L. Wen, H. Yin, W. Li, K. Li, Acta Crystallogr. E 65 (2009) o2623.
[23] P.L. Polavarapu, J. Phys. Chem. 94 (1990) 8106–8112.
[24] J. Karpagam, N. Sundaraganesan, S. Sebastain, S. Manoharan, M. Kurt, J. Raman Spectrosc. 41 (2010) 53–62.
[25] D.A. Kleinman, Phys. Rev. 126 (1962) 1977–1979.
[26] R. Ditchfield, J. Chem. Phys. 56 (1972) 5688–5691.
[27] Y. Ataly, D. Avai, A. Basoglu, Struct. Chem. 19 (2008) 239–246.
[28] T. Vijayakumar, I. Hubert Joe, C.P.R. Nair, V.S. Jayakumar, Chem. Phys. 343 (2008) 83–99.
[29] M. Karabacak, M. Cinar, M. Kurt, J. Mol. Struct. 968 (2010) 108–114.
[30] E. Kavitha, N. Sundarabganesan, S. Sebastian, Indian J. Pure Appl. Phys. 48 (2010) 20–30.
[31] Onkar Prasad, Leena Sinha, Naveen Kumar, J. At. Mol. Sci. 1 (2010) 201–214.
[32] R.G. Parr, L.V. Szentpaly, S.J. Liu, Am. Chem. Soc. 121 (1999) 1922–1924.
[33] P.K. Chattraj, B. Maiti, U.J. Sarkar, J. Phys. Chem. A 107A (2003) 4973–4975.
[34] R.G. Parr, R.A. Donnelly, M. Levy, W.E. Palke, J. Am. Chem. Soc. 68 (1978) 3807.
[35] R.G. Parr, R.G. Pearson, J. Am. Chem. Soc. 105 (1983) 7512–7516.
[36] R.G. Parr, P.K. Chattraj, J. Am. Chem. Soc. 113 (1991) 1854–1855.
[37] (a) R. Parthasarathi, J. Padmanabhan, B. Maiti, P.K. Chattraj, J. Phys. Chem. A 107 (2003) 10346–10352;
(b) P. Thanikaivelan, V. Subramanian, J. RaghavRao, B.V. Nair, Chem. Phys. Let 323 (2000) 59;
(c) R. Parthasathi, J. Padmanabhan, M. Elango, V. Subramanian, P.K. Chattraj, Chem. Phys. Lett. 394 (2004) 225.
[38] R. Parthasarathi, J. Padmanabhan, V. Subramanian, B. Maiti, P.K. Chattraj, Curr. Sci. 86 (2004) 535.
[39] R. Parthasarathi, J. Padmanabhan, V. Subramanian, U. Sarkar, B. Maiti, P.K. Chattraj, Internet Electron. J. Mol. Des. (2003) 798.
[41] M. Arivazhagan, K. Sambathkumar, S. Jeyavijan, Indian J. Pure Appl. Phys. 48 (2010) 716–722.
[42] G. Varsanyi, Assignments for Vibrational Spectra of Seven Hundred Benzene Derivatives, vols. 1–2, Academic Kiaclo, Budapet, 1973.
[43] S. Sebastian, N. Sundaraganesan, B. Karthikeiyan, V. Srinivasan, Spectrochim. Acta A 78 (2011) 590–600.
[44] R.M. Silverstein, C. Bassler, T.C. Morill, Spectrometric Identification of Organic Compounds, fifth ed., John Wiley & Sons, 1991.
[45] A.J.A. Bienko, Z. Latajka, D.C. Bienko, D. Michalska, J. Chem. Phys. 250 (1999) 123.
[46] G. Socrates, Infrared Raman Characteristic Group Frequencies Tables and Charts, third ed., Wiley, ChiChester, 2001.
[47] J. Coates, R.A. Meyers, Interpretation of Infrared Spectra, A Practical Approach, John Wiley & Sons Ltd., Chichester, 2000.
[48] S. Sebastian, N. Sundaraganesan, Spectrochim. Acta A 75 (2010) 941–952.
[49] S. Gunasekaran, R.K. Natarajan, R. Rathikha, D. Syamala, Indian J. Pure Appl. Phys. 43 (2005) 503–508.
[50] M.T. Gulluoglu, S. Yurdakul, Vib. Spectrosc. 25 (2001) 205–211.
[51] M.T. Gulluoglu, S. Yurdakul, J. Mol. Struct. 641 (2002) 93–100.
[52] N. Sundaragnesan, S. Ayyappan, H. Umamaheswari, B.D. Joshua, Spectrochim. Acta A 66 (2007) 17–27.
[53] R. Wysokinski, D. Michalska, D.C. Bienko, S. Ilakiamani, N. Sundaraganesan, K. Ramalingam, J. Mol. Struct. 791 (2006) 70–76.
[54] R.M. Silverstein, F.X. Webster, Spectrpmetric Identification of Organic Compounds, sixth ed., John Wiley & Sons Inc., 1998. p. 102.
[55] N. Sundaraganesan, B. Dominic Joshua, C. Meganathan, R. Meenashi, J.P. Cornard, Spectrochim. Acta A 70 (2008) 376–383.
[56] K. Sambathkumar, Density Functional Theory Studies of Vibrational Spectra, Homo-Lumo, Nbo and Nlo Analysis of Some Cyclic and Heterocyclic Compounds (Ph.D. thesis), Bharathidasan University, Tiruchirappalli, August 2014.
[57] A.E. Reed, F. Weinhold, J. Chem. Phys. 83 (1985) 1736–1740.

Further reading

[40] S. Subashchandrabose, Akhil R. Krishnan, H. Saleem, V. Thanikachalam, G. Manikandan, J. Mol. Struct. 981 (2010) 59–70.